Multiscale and Multidisciplinary Modeling, Experiments and Design (2026) 9:158
https://doi.org/10.1007/s41939-026-01236-4

ORIGINAL PAPER

Towards fluidization in domestic heat systems: a cfd analysis of a fluidized bed cookstove

Nicholas Lwasa[1] · **Ronald Kayiwa**[1] · **Vianney Andrew Yiga**[1]

Received: 9 March 2026 / Revised: 25 May 2026 / Accepted: 4 June 2026

Abstract
Conventional direct combustion and gasifier stoves operate a packed bed combustion technology, which is not favorable for combustion of fine solid biomass such as charcoal fines because of the compact nature of these fuels, which blocks airflow, leading to incomplete combustion. Conversely, fluidized bed combustion technology would effectively combust fine fuels; however, this is largely a monopoly of the industrial sector for processes such as heating, drying, separation, power generation, among others, and has never been adopted in cookstove designs despite its high-quality combustion and heat transfer potential. This study, therefore, presents the design, modeling, and simulation of a fluidized bed cookstove specifically developed for the direct combustion of charcoal dust, without the need for briquetting. The cookstove employed a bubbling fluidized bed combustion mechanism to enhance fuel–air mixing, hence promoting complete combustion and improving heat transfer. The stove design was a result of mathematical modeling using empirical formulae from previous studies. Computational Fluid Dynamics (CFD) was employed to model and simulate both the hydrodynamic behaviour and combustion processes within the reactor, thereby predicting the model performance. The cookstove featured a funnel-shaped combustion chamber with a dense phase region (Ø0.106 m × 0.119 m), a lean phase region (Ø0.212 m × 0.064 m), and a total reactor height of 0.182 m. CFD results indicated dense phase particle concentration with no entrainment and a maximum combustion temperature of 726.8°C.

Keywords Fluidized bed cookstove · Charcoal dust · Fluidization · Computational fluid dynamics

1 Introduction

Biomass resources of both raw (agricultural residues, animal waste, wood) and processed (charcoal, briquettes, pellets) natures make up about 80% of cooking energy in sub-Saharan Africa (Okino et al. May 2021). Direct combustion of solid biomass is the most practical and cost-effective method for domestic cooking (Mukunda and Professor 2022), explaining why most cookstoves are direct combustion rather than indirect combustion or gasifiers (Memon et al. Sep. 2020). Both direct combustion and gasifier stoves, whether forced or natural draft, operate with a packed bed of fuel, where the fuel remains stationary relative to airflow (Sutar et al. Apr. 2017). However, these stoves are suited for medium or coarse fuels, and not fine particle fuels like charcoal dust. Birzer, et al. (2019) observed that larger fuel pieces (D/5) burn longer and more efficiently than smaller ones (D/10). Deng et al. (2018) noted that small particles can block airflow, hinder pyrolysis, extinguish flames, or reduce efficiency due to poor air–fuel ratios. In addition, Tanui et al. (2018) reported that its low durability further limits performance in solid-fuel stoves. Furthermore, works of Hwangdee et al. (2023) revealed that charcoal dust's low bulk density requires frequent refilling compared to lump charcoal. Moreover, low fuel density shortens the combustion period of a fuel (Sen et al. 2016). In spite of the case made for charcoal dust not being suitable for use in existing charcoal stoves, it is continually generated during transportation, storage, and vending, with vendors estimating up to one basin or two tins per bag of charcoal. Of this, about 40% is sold, 31% thrown away, 23% used by vendors themselves (for warming, steaming food, cleaning saucepans, smell control, filling ditches, and construction), and 5% freely given away. The portion sold is mainly used for earth wiring (70%), farming (13%), briquette production (9%), and saucepan repair (9%) (Mugo et al.

✉ Vianney Andrew Yiga
vianney.yiga@mak.ac.ug

[1] Department of Mechanical Engineering, Makerere University, Kampala, Uganda

Published online: 29 June 2026

2016). With a calorific value of 14–30 MJ/kg (Hwangdee et al. 2023) depending on feedstock, charcoal dust presents considerable potential to meet cooking energy needs in developing countries owing to its low cost, wide availability, and high energy content.

On the flip side, fine biomass fuels are well-suited for combustion in fluidized bed combustors due to thorough mixing of the inert bed material, fuel, and fluidizing medium. In this process, fuel is injected into a hot bed of inert material (commonly sand) suspended by an oxidizing medium, such as air or steam, uniformly supplied from the reactor's base (González-Vázquez et al. 2018). Fluidized bed technology is classified by reactor design, which is determined by the fluidizing regime, itself dependent on operating velocity. Two main regimes exist: the bubbling regime, where the bed remains stationary after fluidization, and the circulating regime, where bed material is transported out of the reactor (Zhang et al. 2023). The bubbling fluidized bed (BFB) remains particularly attractive for small-scale reactors due to its simple design, lower operational complexity, and suitability for small-scale domestic systems. Additionally, the energy required to run both the blower and heater can be obtained through several options, i.e., a battery, thermal electric generator (TEG), electricity for households connected to the grid, and solar for off-grid households. Moreover, the energy input required significantly drops once the bed reaches the ignition temperature of the fuel and the heater is turned off. Recent small-scale fluidized bed combustion research has largely focused on gasifier design (Bamido 2018; Hossain et al. 2022; Vargas-Salgado et al. 2021), typically employing a bubbling fluidized bed with sand as the bed material (200–500 μm) and air as the fluidizing agent. There is a growing shift towards renewable biomass fuels such as rice straw, wood pellets, and decaying plant residues to reduce fossil fuel reliance and improve sustainability (Leckner 2019; Rowe and Yates 2020). Bed material properties have been determined through experiments, desk reviews, or blended approaches (Ranzi et al. 2016), with designs relying heavily on empirical correlations from prior studies, alongside design rules and experiments, for instance, in distributor plate design by Vargas-Salgado et al. (Vargas-Salgado et al. 2021). In addition to core components like the combustion chamber, plenum, fuel feeder, and blower, designs often feature a downstream cyclone to prevent solid entrainment (Leckner 2016). Reactor geometries are generally cylindrical, with diameters ranging from 10 to 50 cm and heights from 20 to 170 cm (Hossain et al. 2022; Vargas-Salgado et al. 2021), and stainless steel is the preferred material. Performance evaluation of a design in a bid to reduce costs, development time, allow for early detection of flaws, and improve product quality was dominated by simulations, with occasional use of both simulations and prototypes. Computational fluid dynamics (CFD) dominated most simulations, with reported performance metrics consistently including Cold Gas Efficiency (CGE), Carbon Conversion Efficiency (CCE), syngas yield, and Lower Heating Value (LHV). Recent CFD applications in cookstoves have mainly focused on design optimisation and performance prediction of improved cookstoves (ICS) (Commeh et al. 2022; Dhakare et al. 2025; Husain et al. 2020; Pundle et al. 2019), typically modelling only a single phase (air) since the fuel remained stationary.

Fluidized bed (FB) combustion has been adopted by industrialists for its superior mixing, efficient heat and mass transfer, precise temperature control, reduced pollutant emissions, and enhanced combustion efficiencies (Luo and Tao 2017). Despite these thermal merits combined with fuel flexibility and a variety of modeling techniques, the concept has not been applied to cookstoves. The aim of this study, therefore, was to design a fluidized bed cookstove for direct combustion of charcoal dust and analyse its performance using CFD. In this study, CFD modeling examined multiphase flow, i.e., for both solid and gas phase behaviour in a fluidized bed cookstove (FBC).

2 Materials and methods

2.1 Material selection

The materials whose properties were of interest during this study were: bed material, fuel, and fluidizing medium. While sand was the prevalent bed material in previous studies (Bamido 2018; Hossain et al. 2022), this study considered only naturally occurring sand, from which several types were shortlisted. The final choice of sand was made following a material selection matrix (see Table 1).

Notably, sand is a typical Geldart group B particle whose diameter ranges from 40 to 500 microns according to Duan and Lu (2025) and is deemed optimal for fluidization due to its ease of fluidization and minimal inter-particle cohesion. Patel et al. (2021) defined even a wider range of group B particles, i.e., 150 to 1000microns. However, various studies agree that silica sand tends to have volume changes when it reaches 573°C, and this is largely due to the high level of SiO_2 in the sand sample. Though Svidró et al. (2020) argued that other than temperature, the size of the sand particles is another factor that affects thermal expansion, with particles in the range of (0.355–0.5 mm) showing higher expansion than particles in the range of (0.25–0.335 mm) of the same silica sand type. Against that background, sand particles of 300microns and 200microns were both suitable for selection in this study, though, ultimately, the 200micron particles were chosen since they would require less energy to fluidize. However, the available sieves at the laboratory within this range

Table 1 Bed material selection matrix

Selection Criteria	Silica	Zirconium	Raw Sands Kerphalite KF (Andalusite)
Shape	0	0	0
Size distribution (m)	+	+	–
Surface roughness	+	–	–
Rigidity	–	0	0
Attrition resistance	–	0	0
Particle density (kg/m^3)	0	–	–
Bulk density (kg/m^3)	0	–	–
Melting point (^0C)	0	+	+
Linear expansion coefficient	0	+	+
Specific heat capacity J/(kg ^0C)	+	–	–
Sum of + 's	3	3	2
Sum of 0's	6	3	3
Sum of – 's	2	4	5
Net score	1	−1	−3
Rank	1	2	3
Rank	1	2	3

were 212 μm and 300 μm, and the average size was used for this study.

From Table 1, a sample of plaster and lake sand, purportedly rich in silica, was collected from Bweyogerere sand landfill in Wakiso district (latitude 32.66º, longitude 0.35º), about 10 km from Kampala City center. The samples were oven-heated at 100°C for 24 h to determine moisture content. Sieve analysis yielded sand with an average particle size of 256 μm, which was tested for physical and chemical composition. Particle density was determined by the pycnometer method, porosity by the porosity method, and chemical composition via XRF spectrometry. Physical and chemical properties of the charcoal species used in the design and CFD modeling were from Lubwama et al. (2023) and elemental properties from Dran (2025). The study used 1.77 mm charcoal dust particles, as most available particles are under 2 mm (Al 2013). The fluidizing medium was air with its physical and thermal properties taken from Marinos-Kouris and Maroulis (2024).

2.2 Design parameters

The design parameters that were considered for efficient and optimum design included geometry and operating parameters, which were determined through mathematical modeling using empirical formulae, design rules, and assumptions from previous studies on fluidization and cookstove design (Vargas-Salgado et al. 2021; Grace et al. 2020; Sweeney 2017). The appropriate design parameters of the fluidized bed cookstove (FBC) were determined as follows:

2.2.1 Minimum fluidization velocity

The minimum fluidization velocity, which is the superficial gas velocity at which the fluidization of the particles is initiated, u_{mf}, was determined using Eq. 1**,** whereas Archimedes' number, Ar, was determined using Eq. 2 (Grace et al. 2020). Equation 1, also known as the Wen and Yu correlation, is suited for Geldart B particles such as sand, but not for very fine and coarse particles. However, it assumes that bed particles are completely spherical, which is not always the case (Anantharaman et al. 2018; Cáceres-Martínez et al. 2023).

$$u_{mf} = \frac{\mu}{\rho_f d_p}\left[\sqrt{\{33.7^2 + 0.0408Ar\}} - 33.7\right] \quad (1)$$

$$Ar = \frac{\rho_f g(\rho_p - \rho_f){d_p}^3}{\mu^2} \quad (2)$$

where μ is the viscosity of air, ρ_f is the density of air, ρ_p is the density of a sand particle, d_p is the diameter of a sand particle, and g is the acceleration due to gravity.

2.2.2 Operating velocity

The operating velocity is the velocity at which the bed will constantly operate. This is normally more than the minimum fluidization velocity and less than the terminal settling velocity. The operating velocity, $U_{f,}$ was determined using Eq. 3 (Mota 2015). Where, $1.2 < \frac{H}{H_{mf}} < 1.4$ for bubbling fluidized beds (Grace et al. 2020). For this study, a value of 1.3 was considered. Equation 3 is suited for bubbling fluidized beds and not smooth fluidization. However, it assumes uniform bed expansion, which is normally unlikely (Balag et al. 2023).

$$\frac{H}{H_{mf}} = 1 + \frac{10.978(U_f - u_{mf})^{0.738}{\rho_p}^{0.376}{d_p}^{1.006}}{{u_{mf}}^{0.937}{\rho_f}^{0.126}} \quad (3)$$

where H is the packed bed height, and H_{mf} is the minimum fluidization height.

2.2.3 Terminal settling velocity

The terminal settling velocity, $V_{t,}$ is the constant velocity that is reached by a particle falling through a considerable distance in a stagnant fluid. It is therefore the maximum speed at which the fluidization process can take place without carrying the particles out of the reactor. The terminal velocity, V_t, was determined from Eq. 4 (Grace et al. 2020). However, before

that, the dimensionless particle diameter, d_p^* and dimensionless terminal velocity, V^*_t were determined from Eqs. 5 and 6, and sphericity ϕ was considered as 0.86 for this study (Grace et al. 2020). Equation 4 is suited for gas–solid systems. However, its accuracy depends on the sphericity, since particles aren't truly spherical (Goossens 2019; Kalman and Matana 2022).

$$V^*_t = V_t \times \left\{ \frac{{\rho_f}^2}{\mu g\left(\rho_p - \rho_f\right)} \right\}^{1/3} \tag{4}$$

$$d_p^* = d_p \times \left\{ \frac{\rho_f g\left(\rho_p - \rho_f\right)}{\mu^2} \right\}^{\frac{1}{3}} \tag{5}$$

$$V^*_t = \left[\frac{18}{{d^*_p}^2} + \frac{(2.3348 - 1.7439\phi)}{{d^*_p}^{0.5}} \right]^{-1} \tag{6}$$

2.2.4 Energy needed

This was determined based on a 3L pot. Given the mass of water (M_w) to be 3000 g, the specific heat capacity of water (Cp_w) to be 4.186 J/g°C, and the time, t taken to raise the temperature of water (ΔT) from 25°C to 100°C at sea level to be 10 min, the power requirement,Q of the stove was determined from Eq. 7 (Getahun et al. 2019).

$$Q = \frac{M_W Cp_w \Delta T}{t} \tag{7}$$

2.2.5 Fuel consumption rate

The fuel consumption rate (FCR) was determined from Eq. 8 (Getahun et al. 2019), considering the average calorific value (HHV) of the charcoal to be used from literature to be 28.586 MJ/kg (Lubwama et al. 2023), and assuming the stove to operate at Tier 3 thermal efficiency (η_{th}), i.e., 35%. The stove was assumed to be Tier 3 because it is the average rating for most improved cookstoves (Champion et al. 2021; Yunusa et al. 2023).

$$FCR = \frac{Q}{HHV\eta_{th}} \tag{8}$$

2.2.6 Volumetric flow rate

The volumetric flow rate of the air ($\dot{Q}_{air}$) was determined using Eq. 9 (Vargas-Salgado et al. 2021), with the Equivalent ratio (ER) considered as 1 since the reactor was designed to achieve complete combustion other than gasification (ER<1), where, the stoichiometric fuel ratio (γ) using Eq. 10 (Vargas-Salgado et al. 2021), with values of C, H and O determined from the ultimate analysis of the charcoal from previous studies (Dran 2025).

$$\dot{Q}_{air} = FCR\gamma ER \tag{9}$$

$$\gamma = \frac{137.3}{\rho_{air}}\left(\left(\frac{Mass_C}{12.011} + \left(\frac{1}{4}\frac{Mass_H}{1.008}\right)\right) - \frac{Mass_O}{32}\right) \tag{10}$$

2.2.7 Diameter of the reactor

The area of the reactor, A_R, was determined using Eq. 11 from Vargas-Salgado et al. (2021), and subsequently, the dense phase diameter section, d_R (lower section of the combustion chamber), was determined from Eq. 12.

$$A_R = \frac{\dot{Q}_{air}}{U_f} \tag{11}$$

$$d_R = \sqrt{\left(\frac{4A_R}{\pi}\right)} \tag{12}$$

The diameter of the lean phase section (top section of the combustion chamber) is also required to be a low velocity zone, d_{lv}, to reduce the drag on the sand and char, thereby reducing entrainment, which was determined using Eq. 13 (Vargas-Salgado et al. 2021). The ratio was chosen to be 2 to cater for the average size of a saucepan of 0.24 m and to minimize the fabrication cost. Despite a recommended range of 1–3 (Grace et al. 2020).

$$d_{lv} = 2d_R \tag{13}$$

2.2.8 Height of the reactor

The height of the bubbling bed section, H_{bed}, was determined using Eq. 14 (Vargas-Salgado et al. 2021). The volume of fluid bed, $Vol_{fluidbed}$ determined from Eq. 15. After which the freeboard section H_{fb}, low velocity zone H_{lvz}, truncated cone H_{tc}, intake fuel system H_{is}, and the total height of the reactor H_T were subsequently determined using Eqs. 16, 17, 18, 19, and 20, respectively (Vargas-Salgado et al. 2021). The coefficients used are from empirical design ratios and not fundamental laws. They are informed by experimental observation of bubbling beds (Ganguli and Bhatt 2023; Wytrwat et al. 2020).

$$H_{bed} = \frac{Vol_{fluidbed}}{A_R} \tag{14}$$

$$Vol_{fluidbed} = \frac{Vol_{fixedbed}}{\left(1 - \varepsilon_{mf}\right)} \tag{15}$$

$$H_{fb} = 0.3H_{bed} \tag{16}$$

$$H_{lvz} = 0.7H_{bed} \tag{17}$$

$$H_{tc} = \frac{H_{lvz}}{4} \tag{18}$$

$$H_{is} = \frac{H_{bed}}{3} \tag{19}$$

$$H_T = H_{bed} + H_{fb} + H_{lvz} + H_{tc} + H_{is} \tag{20}$$

2.3 Design description

The FBC comprised a combustion chamber with two regions, i.e., the lean and dense phase sections, a distributor plate for uniform air distribution and complete fluidization, a screen to prevent weeping of bed materials, and a plenum housing the air inlet nozzle (see Fig. 1). Auxiliaries included a blower for supplying fluidizing and primary combustion air, a heater to raise air temperature for heating the bed to charcoal's ignition temperature (400 °C), a thermocouple for bed temperature readings, and an electrical control mechanism for switching the FBC heater or blower and indicating when to add charcoal dust to the combustion chamber (see Fig. 2).

The FBC operates by plugging it into an AC socket (190–240 V), adding 25 g of sand to the combustion chamber, and placing the cooking pot with food on the pot holder. The blower and heater are then switched on. When the sand bed temperature reaches 400 °C, a sound alarm prompts the user to turn off the heater and either add fuel to the hopper or open the hopper valve if fuel is already loaded. The first fuel particle ignites upon contact with the hot sand bed, initiating combustion and heat transfer to the pot. Firepower is regulated either by adjusting the hopper valve or by controlling the fluidizing gas velocity via the blower speed controller (see Fig. 2).

2.4 Computational fluid dynamics modeling

2.4.1 Geometry and meshing

The CFD modeling was divided into the hydrodynamics model and the combustion model. The SolidWorks ® three-dimensional (3D) model of the FBC (see Fig. 1) whose dimensions were from design parameters in subSects. 2.2.7 and 2.2.8 was simplified into a 2D computational domain using Ansys design modeler to reduce computational cost (see Fig. 3A). The models were then meshed using ANSYS® Workbench meshing tool (see Fig. 3B and C) to allow the computer to analyze the result in a more precise way.

2.4.2 Numerical modeling

To model the hydrodynamics of the gas and solid phases, mass, momentum, and energy conservation were defined following the Eulerian-Eulerian model (Sahoo and Sahoo 2015), and these were closed using constitutive equations, i.e., stress tensors, bulk viscosity, shear viscosity, solid pressure, radial distribution function, and granular temperature (Gosavi et al. 2018). The turbulent conditions expected in this study were accounted for using the shear-stress transport (SST) k-ω turbulence model, consisting of two separate transport equations for turbulent kinetic energy and specific dissipation rate. The turbulent kinetic energy, k, and ω, its specific dissipation rate, were obtained through transport Eqs. 21, 22 (Adanta et al. 2020), and the Syamlal-O'Brien drag model was adopted.

$$\frac{\partial(\rho_m k)}{\partial t} + \frac{\partial}{\partial x_i}(\rho_m v_i k) = \frac{\partial}{\partial x_j}\left(\left(\mu + \frac{\mu_t}{\sigma_k}\right)\frac{\partial k}{\partial x_j}\right) + G_k - Y_k + S_k \tag{21}$$

$$\frac{\partial(\rho_m \omega)}{\partial t} + \frac{\partial}{\partial x_i}(\rho_m v_i \omega) = \frac{\partial}{\partial x_j}\left(\left(\mu + \frac{\mu_t}{\sigma_\omega}\right)\frac{\partial \omega}{\partial x_j}\right) + G_\omega - Y_\omega + D_\omega + S_\omega \tag{22}$$

where G_ω represents the generation of ω, G_k represents the generation of k due to mean velocity gradients. Y_ω and Y_k represent the dissipation of ω and k due to turbulence, and D_ω represents the cross-diffusion term. S_ω and S_k are user-defined source terms. In addition, σ_k and σ_ω are the inverse turbulent Prandtl numbers for k and, respectively, ρ_m is the mixture density, v is the mixture velocity, and μ_t is the turbulent viscosity. The combustion model, on the other hand, will follow heterogeneous reactions of char with gas species since the fuel (charcoal dust) is a residue from the pyrolysis of wood. The heat transfer to the cooking pot will be by conduction (between the combustion chamber inner walls and the pot's external walls), convection (via flue gases), and radiation (from the glowing char). The simplified reaction models of char were presented by Ismail et al. (Ismail 2016).

2.4.3 Stove model assumptions

The computational domain for simulation was simplified in a form usable by a computer (see Fig. 3: (A) Combustion model geometry, (B) meshed hydrodynamic model, and (C) meshed combustion model A). Also, the stove was assumed to have a maximum combustion temperature of 900°C, which was based on the operating range for fluidized bed combustion technology, i.e., 650°C–930°C (Scala Mar. 2018). Attrition, segregation, and agglomeration, if any, were neglected.

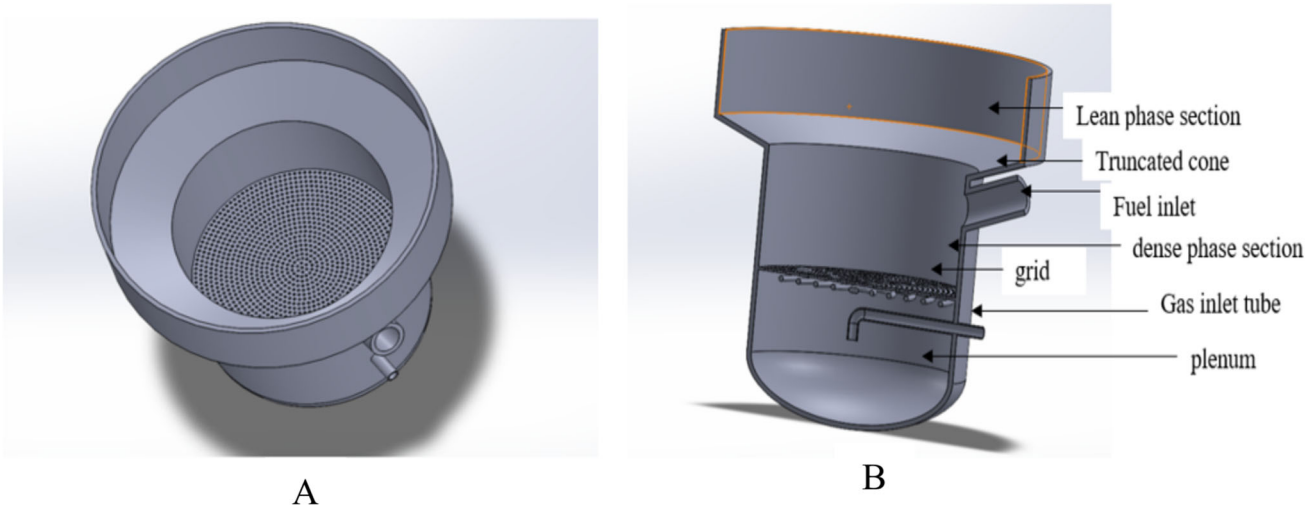

Fig. 1 **A** and **B** are aerial and sectional views of the reactor, respectively

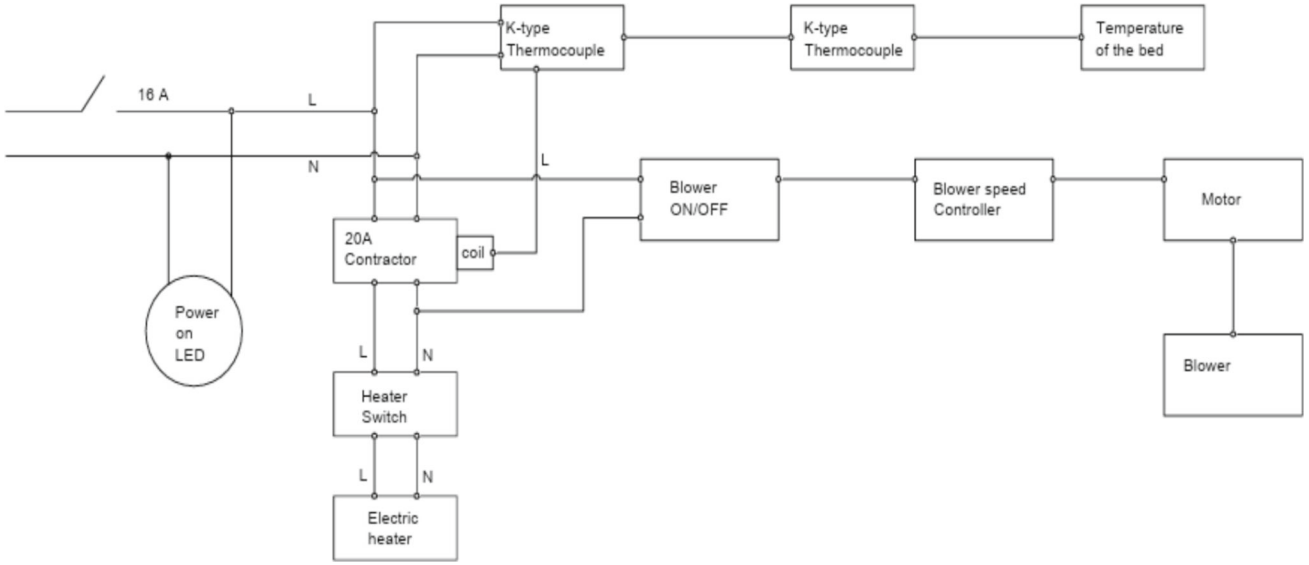

Fig. 2 Electrical circuit schematic of the control mechanism

2.4.4 Stove model boundary conditions and solver settings

The boundary conditions were determined from the mathematical modeling (for operating parameters, i.e., velocity, mass flow rate), and others were estimated from previous studies (Leckner 2019; Grace et al. 2020). The boundary conditions for both models were defined as in Table 2, and subsequently set up as shown in Fig. 4. The Pressure-based solver (PBS) in ANSYS® FLUENT student version 2024 was utilized in this study because it is applicable for a wide range of flow regimes from low-speed incompressible flow to high-speed compressible flow (Commeh et al. 2022).

2.5 Model validation

In this study, CFD simulation results were validated against previous findings on sand-air interaction and biomass combustion (Rowe and Yates 2020; Khezri et al. 2019; Kumar and Agarwal 2016; Li and Eri 2023; Rao et al. 2018; Sadri Mofakham and Rasteh 2023). However, future work is necessary to include experimental validation through prototype testing.

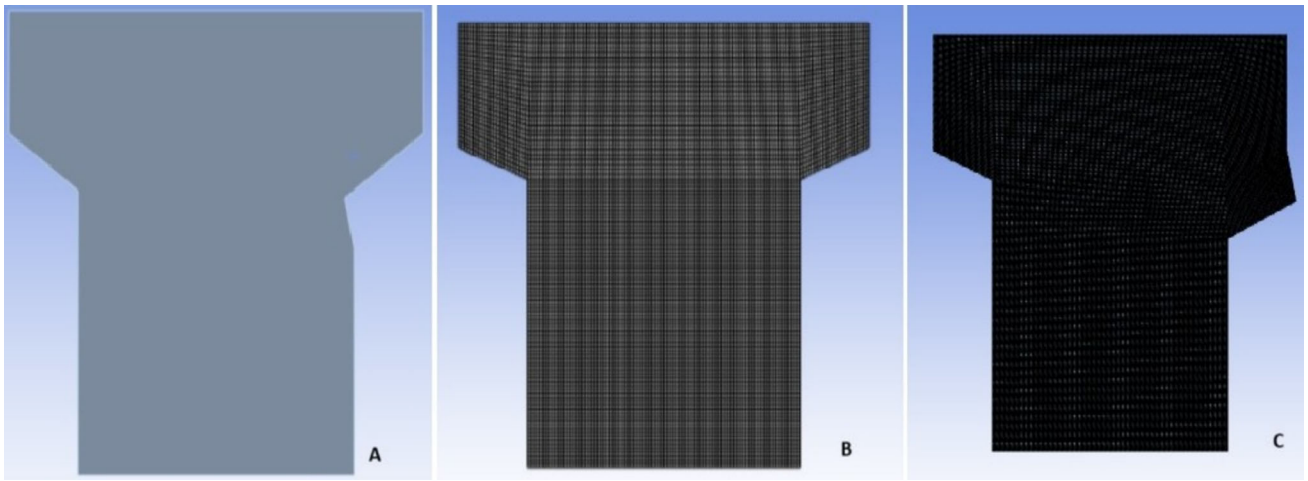

Fig. 3 **A** Combustion model geometry, **B** meshed hydrodynamic model, and **C** meshed combustion model

Table 2 Hydrodynamic and combustion model boundary conditions

Hydrodynamic model		
Location	Metric	Value
Inlet	Phase Velocity (m/s) Temperature (K)	Gas 0.185 300
Internal fluid domain	Phase	Mixture
Outlet	Phase Gauge pressure (Pa)	Mixture 0
Walls	Phase Roughness height (m)	Mixture 0
Combustion model		
Air Inlet (velocity inlet)	Phase Velocity (m/s) Temperature (K)	Gas 0.185 673
Fuel inlet (Mass flow inlet)	Phase Mass flow rate (kg/s) Temperature (K)	Solid 0.0001569 298.15
Internal fluid domain	Phase	Mixture
Outlet (pressure outlet)	Phase Gauge pressure (Pa) Temperature (K)	Mixture 400,000 1200
Walls	Phase Roughness height (m)	Mixture 0

3 Results and discussion

3.1 FBC bed material selection and properties

Both samples of plaster (brown) and lake (white) sand were highly rich in silicon dioxide, i.e., 96.74% and 96.69%, respectively (see Table 3), falling within the typical 90–99.65% range for silica sand (Svidró et al. 2020; Davenport et al. 2020; Wang 2014).

Physically (see Table 3), plaster sand had a particle density of 2666.67 kg/m^3 and lake sand 2631.58 kg/m^3, values comparable to 2650 kg/m^3 reported by Svidró et al. (2020) for sand of 0.25–0.355 mm size. The slightly higher density of plaster sand is linked to its higher Fe_2O_3 content (0.83%) compared to lake sand (0.66%). While the lower-density lake sand might be expected to have higher porosity, the opposite was observed with plaster at 62.5% and lake at 54%. As (Mukhopadhyay et al. 2019) explained, this is due to grain shape: plaster's angular grains pack less efficiently, leaving

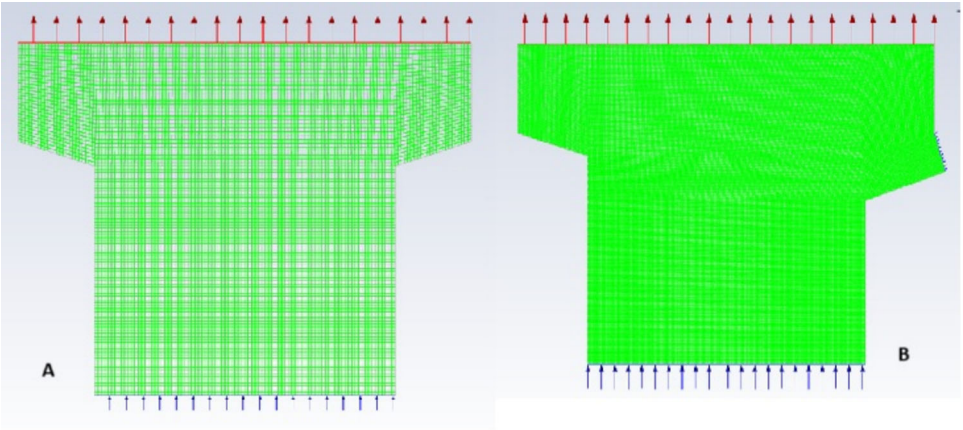

Fig. 4 Boundary conditions setup of **A** the hydrodynamic model and **B** the combustion model

Table 3 Physical and chemical properties of the sand samples

Physical metric	Samples	
	Plaster sand	Lake sand
Moisture content (%)	13.5 ± 1.2	9.6 ± 1.1
Colour	Brownish	Whitish
Particle density (kg/m^3)	2666.67 ± 0.02	2631.58 ± 0.02
Particle size (μm)	256	256
Porosity %	62.5 ± 2.12	54 ± 1.41
Chemical composition		
Al_2O_3%	2.57 ± 0.1	2.47 ± 0.1
Cr_2O_3%	0.02 ± 0.001	0.01 ± 0.001
MnO_2%	0.01	0.01
Fe_2O_3%	0.83 ± 0.001	0.66 ± 0.002
SiO_2%	96.74 ± 0.001	96.69 ± 0.001

more voids, whereas lake sand's rounded grains pack more tightly. For the simulation, lake sand was selected for its lower particle density, which would require a lower velocity to fluidize.

Table 4 Design, operating, and geometry parameters

Design parameters	Design power (kW)	1.57
	Fuel feed rate (kg/s)	0.0001569
	Stoichiometric ratio (m^3/kg)	12.716
	Volumetric flow rate (m^3/s)	0.002
Operating parameters	Minimum Fluidization Velocity, U_{mf}	0.056
	Operating fluidization Velocity, U_f	0.216–0.345
	Terminal Velocity, U_t	1.818
Geometry parameters	Bubbling fluidized bed height	0.073
	Free board height	0.022
	Fuel intake height	0.024
	Truncated height	0.013
	Low velocity zone height	0.051
	Total reactor height	0.182
	Inner reactor diameter	0.106
	Low velocity zone diameter	0.212

3.2 FBC design, operating, and geometry parameters

The design specifications (see Table 4) indicate the FBC was designed with a fire power of 1.57 kW, exceeding conventional cookstove ratings (0.4–1.5 kW) but below the 2–2.5 kW of forced draft rocket stoves reported by Bhatt (Bhatt 2025). The fuel feed rate of 0.56 kg/h falls within the range for 1–2 kW stoves operating in either batch or continuous mode, as noted by Jetter et al. (Jetter et al. 2012). The stoichiometric air–fuel ratio of 12.716 m^3/kg, higher than literature values of 1.6–2 m^3/kg, is likely due to the difference in feedstock elemental composition. Nonetheless, forced draft cookstoves typically operate with excess air to reduce products of incomplete combustion (PICs) (Tariku Woldesemayate and Atnaw 2020). The volumetric flow rate of 0.002 m^3/s lies within the forced draft cookstove norm of 0.00138–0.00833 m^3/s (Hayyat et al. 2024). The FBC operating parameters (see Table 4) indicate a minimum fluidization velocity of 0.056 m/s, consistent with Shao et al. (Shao et al. 2020), who reported 0.05 m/s for sand particles between 0.25–0.3275 mm. The operating velocity for this study was 0.216–0.345 m/s, aligning with the rule of thumb of four times the minimum velocity (Grace et al. 2020). Compared to the terminal velocity of 1.818 m/s, this indicated the bed could operate at 32 times the minimum velocity with little or no entrainment, providing flexible operating parameters and making the design easier to run with less precision. The geometrical parameters of the FBC are summarised in Table 4 and compared with existing direct combustion stoves

as follows. Natural-draft rocket stoves typically have combustion chamber diameters of 0.08–0.12 m and depths of 0.135–0.175 m, while forced-draft types, with higher airflow and firepower, use larger dimensions of 0.12–0.18 m diameter and 0.30–0.37 m height (Boafo-Mensah et al. 2020; Jani et al. 2020; Obi et al. 2020; Still et al. 2015). The modeled FBC had a non-uniform diameter, making direct diameter comparison difficult, and a smaller height of 0.182 m, reflecting its lower firepower of 1.57 kW compared to forced draft stoves (2–2.5Kw) (Still, et al. 2021). Its height-to-diameter ratio met literature recommendations of 1.3–2.5 to enhance residence time and reduce PICs (Sedighi and Salarian 2017). Both model and literature findings emphasise that optimal geometry depends on fuel type, combustion mode, chamber shape, and pot configuration (Lahai et al. 2022), and not a one-size-fits-all solution.

3.3 CFD modeling results

Computational fluid dynamics modeling was conducted to visualize the solid–gas mixing and combustion process, enabling observation of fluidization quality and temperature contours within the chamber.

3.3.1 Mesh quality

The mesh quality of the combustion and hydrodynamic models was compared with the acceptable ranges specified in the ANSYS FLUENT 12.0 User's Guide—6.2.2 Mesh Quality ("ANSYS FLUENT 2025). The mesh statistics attained were aspect ratios of 1.0921 and 1.2273 for the hydrodynamic and combustion model, respectively, both well below the recommended aspect ratio of < 5. Orthogonal quality was 0.99754 and 0.99074 for hydrodynamic and combustion, respectively, both within the recommended range of 0.95–1. The elemental quality was 0.99006 and 0.96106 for both hydrodynamic and combustion, respectively, both greater than the recommended > 0.7 (Sadri Mofakham and Rasteh 2023).

3.3.2 Monitor plots

The graphical representation of the calculation process is illustrated in Fig. 5.

This was meant to show the progress of the solution and whether or not there was convergence.

The monitored residuals included continuity, particle and gas velocity, turbulent kinetic energy, specific dissipation rate, and volume fraction. Over 1600 iterations were performed to resolve the nonlinear terms, with residuals initially turbulent but stabilizing upon fluidization, in agreement with (Sahoo and Sahoo 2015; Kumar and Agarwal 2016; Gamal et al. 2024). The attainment of a steady state across all residuals confirmed convergence and solution stability, further indicating complete fluidization of the bed (Ismail 2016; Askaripour 2020).

3.3.3 Particle concentration

Initially, the inert sand bed of 256 μm particle size was at rest (see Fig. 6A). As the air velocity increased from 0 m/s to the minimum fluidization velocity of 0.056 m/s, voids (air bubbles) began to form since sand is a Geldart B particle, which is bubble ready (Bakshi et al. 2017). Further increase in the air velocity expanded the bed up to the end of the dense phase section, at which point the bed was also fully fluidized (see Fig. 6B). The Sand particles were fluidized by air at a uniform velocity of 0.185 m/s, a value between the minimum fluidizing velocity and the operating velocity, consistent with Luo & Tao (Luo and Tao 2017). No sand particles were blown out of the low-velocity zone (see Fig. 6B), indicating the bed should not be loaded with more sand than specified in the design and can be operated over time with the same sand quantity. A lag exists between the first and last particles to fluidize, so the bed should be allowed sufficient time for complete fluidization, as surface particles fluidize before those in contact with the distributor plate. Figure 6 shows particle concentration predominantly in the dense phase section. This is consistent with the findings of Leckner (Leckner 2019) and Grace et al. (Grace et al. 2020), who recommended concentration dominance in the lower section. The near-zero volume fraction close to the distributor plate implies uniform fluidization, as reported by Pang et al. (Pang et al. 2021). The absence of solids in this region, followed by a drop to zero in the lean dense section, confirms that the bed has reached maximum expansion height, a typical behaviour of gas–solid fluidized beds using the Syamlal-O'Brien model (Khezri et al. 2019). This uniform bed expansion reflects a uniform pressure gradient above the distributor plate, driven by the uniform kinetic energy of air through the orifices (Beheshti et al. 2015). This validated the no segregation assumption. As the pressure drop effect diminished and a steady state was reached, this meant that complete fluidization was achieved, making the bed ready for biomass injection.

3.3.4 Temperature contours

The maximum combustion temperature reached was 1000 K (726.85°C) (see Fig. 7). This was quickly reached because when the fresh biomass (charcoal dust) is injected into the bed, it immediately mixes with the bed material due to the intense gas–solid momentum exchange, resulting in a significant heat and mass transfer, which sharply increases the bed operating temperature as a result of biomass combustion (Kwong and Marek 2021). Kong et al. (Kong et al. 2022) reported that increasing the bed operating temperature in turn increases the temperature difference between the biomass

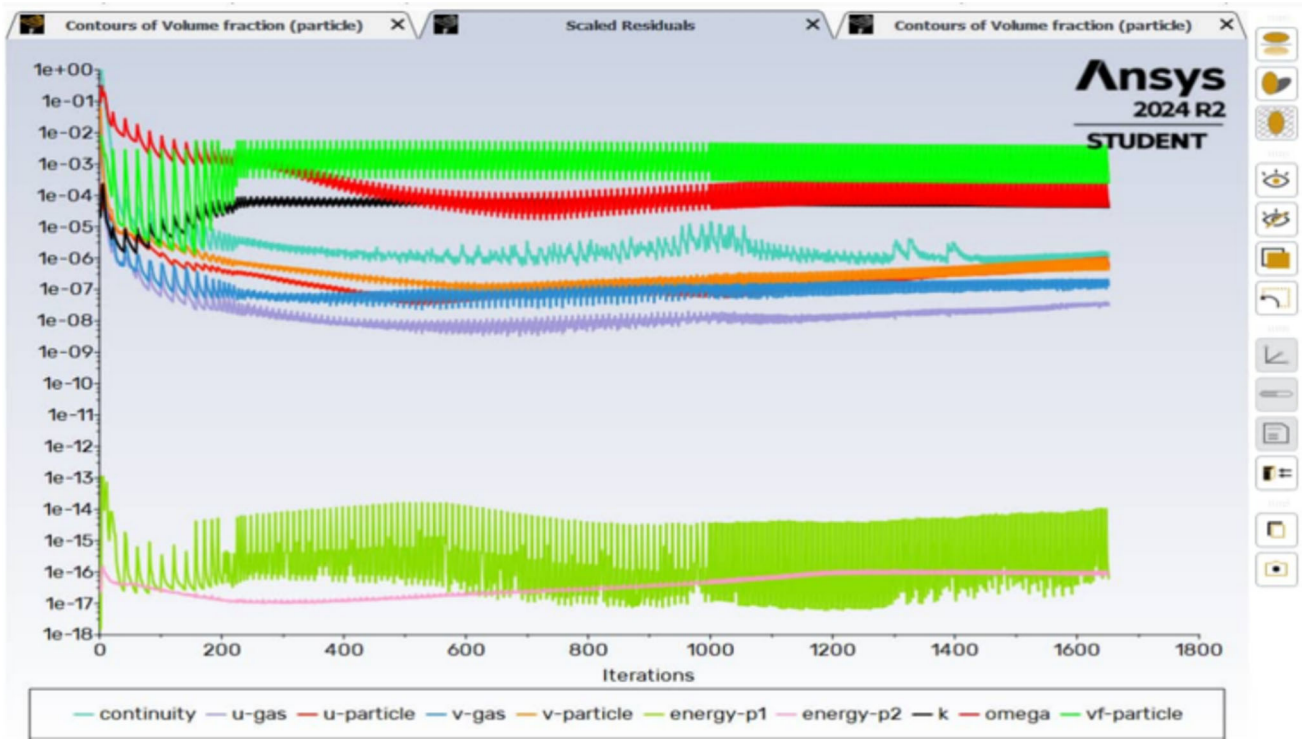

Fig. 5 Velocity, energy, volume fraction, and turbulence profiles

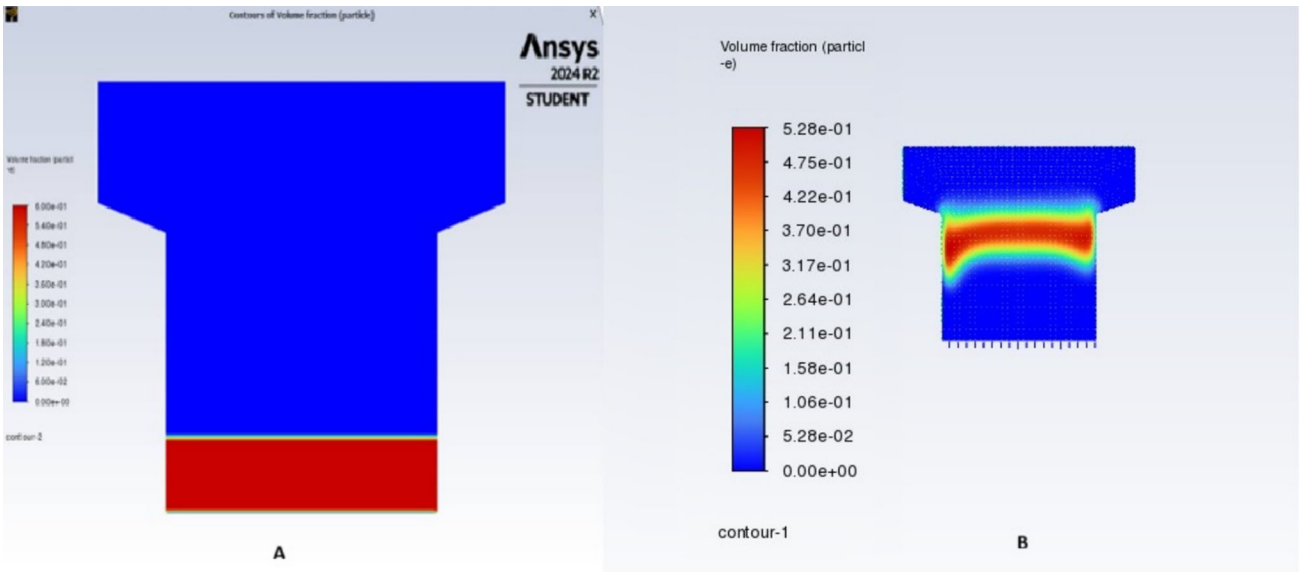

Fig. 6 **A** Particle concentration before fluidization and **B** particle concentration upon achieving fluidization and maximum bed expansion

particle and the gas-sand temperature, leading to intense heat exchange, which in turn increases the biomass temperature. However, Shabanian and Chaouki (Shabanian and Chaouki 2017) advised that the bed temperature should be increased cautiously since this can reduce the density of the gas and thus reduce heat transfer by convection. The maximum combustion temperature fell within the typical range for fluidized bed combustors (650 to 930°C) (Vargas-Salgado et al. 2021; Scala 2018). This temperature is ideal for both cookstove use and fluidized bed combustion, as it exceeds the auto-ignition temperature of CO (609°C) (Sweeney 2017) while remaining below the ash agglomeration temperature of 800–850°C according to Rowe and Yates (Rowe and Yates 2020). The fuel inlet and distributor plate are cooler regions, which is desirable for equipment and user safety; moreover, the maximum temperature was at the stove outlet, which increases

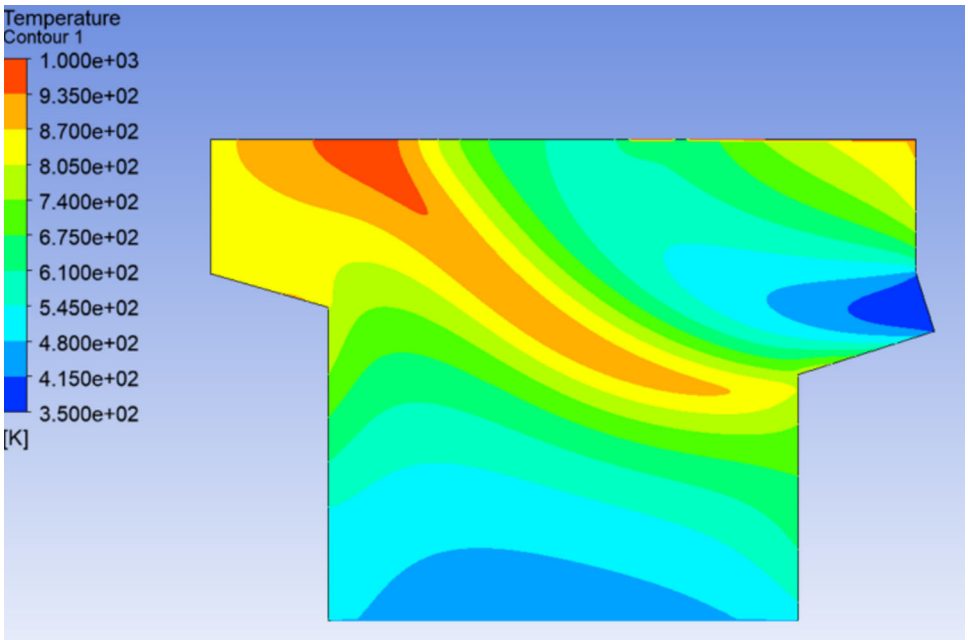

Fig. 7 Temperature distribution in the reactor

radiative heat transfer, an ideal scenario for cookstove designers.

3.4 Model validation

The minimum fluidization velocity obtained by mathematical modeling was 0.056 m/s, falling within the reported range for sand-air fluidized beds of 0.05–0.065 m/s (Kumar and Agarwal 2016; Rao et al. 2018; Sadri Mofakham and Rasteh 2023). The superficial gas velocity applied was 0.185 m/s, lower than the 0.25 m/s and 0.38 m/s used by Kumar & Agarwal (Kumar and Agarwal 2016) and Sadri Mofakham & Rasteh (Sadri Mofakham and Rasteh 2023), respectively, likely due to their larger sand particle sizes (300 μm and 275 μm). Nevertheless, it was within the 0.025–0.51 m/s range for sand-air beds (Rao et al. 2018). Uniform bed expansion (see B) was achieved through consistent kinetic energy of air across the 2 mm distributor orifices, as predicted by Khezri et al. (Khezri et al. 2019) for orifice sizes between 2 and 5 mm. Bubble formation at incipient fluidization confirmed the expected behaviour of Geldart group B particles (Grace et al. 2020), consistent with Rowe and Yates (Rowe and Yates 2020). The observed temperature profile and maximum combustion temperature of 726 °C also matched the 720–820 °C range reported in CFD-DEM simulations (Li and Eri 2023).

4 Conclusions

The FBC was successfully designed and performance simulated using ANSYS FLUENT. This research was done by considering the design of a cookstove, which would be fuelled using charcoal dust, a readily available resource in communities across developing countries. The main conclusions are:

The size of the combustion chamber was obtained through mathematical modeling. The funnel-like combustion chamber featured a dense phase region (Ø0.106 m × 0.119 m), a lean phase region (Ø0.212 m × 0.064 m), and a total reactor height of 0.182 m. The operating velocity of the FBC was also obtained through empirical formulae on fluidization, which was 0.185 m/s. The 3D model of the reactor design was accurately produced using SolidWorks® and imported into Ansys Fluent® (CFD) to simulate the model's performance during operation. The model predicted smooth fluidization and zero entrainment of the bed materials and a maximum combustion temperature of 726°C, which falls within the established operating range for fluidized bed combustors (650–930 °C).

4.1 Limitations of the study

Several methodological limitations of this study are explicitly acknowledged. The combustion process was not fully characterized; in particular, the products of combustion were not resolved in FLUENT, and it is recognized that CFD-predicted combustion species concentrations typically exhibit considerable variance relative to experimental measurements. Furthermore, three key fluidized bed phenomena; agglomeration, segregation, and attrition were not modelled. Agglomeration was excluded on the basis that the predicted maximum combustion temperature (726.85 °C) remained below the 800–850 °C threshold associated with the onset of ash agglomeration. Segregation was neglected because the

bed material was prepared through sieve analysis to yield a near-uniform particle size, and segregation is primarily driven by particle size disparity. Attrition was considered negligible given the small bed mass employed (25 g), which is readily replenishable in the event of particle shrinkage.

A formal grid independence analysis was not performed, as uniform air distribution was assumed at the pressurized inlet during modelling (see Fig. 4), and mesh quality was instead confirmed against ANSYS FLUENT acceptability thresholds (aspect ratio < 5; orthogonal quality 0.95–1; elemental quality > 0.7). Nevertheless, the sensitivity of results to mesh refinement was not systematically quantified, and a structured convergence study is recommended in future work. Additionally, CFD model validation was conducted exclusively through comparison with previously published studies employing similar bed material properties and particle sizes, rather than against experimental data from a prototype of the present design. While the predicted minimum fluidization velocity (0.056 m/s), bed hydrodynamics, and combustion temperature showed satisfactory agreement with reported literature ranges, the absence of experimental validation for this specific geometry and operating condition represents a recognized limitation of the current study.

4.2 Future work

Based on the above, the construction and testing of a physical prototype is strongly recommended to experimentally validate the model results, verify the simplifying assumptions adopted, and evaluate the stove's thermal efficiency and emissions performance under real operating conditions.

Author contribution NL was involved in Conceptualization, Data analysis, Writing-original draft, Technical editing, Fund acquisition. RK was involved in Writing-original draft, Technical editing, Supervision, Investigation. VAY was involved in Conceptualization, Writing-original draft, Technical editing, Supervision, Fund acquisition, Investigation.

Funding No specific funding was received for this work.

Data availability Data related to this manuscript is available from the corresponding author upon reasonable request.

Declarations

Conflict of interest The authors declare no competing interests.

Ethical approval and informed consent statement The study did not involve any animals or participants.

References

"ANSYS FLUENT 12.0 User's Guide - 6.2.2 Mesh Quality." Accessed: Mar. 16, 2025. [Online]. Available: https://www.afs.enea.it/project/neptunius/docs/fluent/html/ug/node167.htm

D. Adanta, I. M. R. Fattah, and N. M. Muhammad, (2020) "Comparison of standard k-ε and SST k-ω turbulence model for breastshot waterwheel simulation,".

A.-R. R. S. Al, "Influence Of Adhesive Type and Particle Size On Compressed Charcoal Briquettes Manufacturing," 2013.

Anantharaman A, Cocco RA, Chew JW (2018) Evaluation of correlations for minimum fluidization velocity (Umf) in gas-solid fluidization. Powder Technol 323:454–485

Askaripour H (2020) CFD modeling of gasification process in tapered fluidized bed gasifier. Energy 191:116515. https://doi.org/10.1016/j.energy.2019.116515

Bakshi A, Ghoniem AF, Altantzis C (2017) Mixing dynamics in bubbling fluidized beds. AIChE J 63(10):4316–4328. https://doi.org/10.1002/aic.15801

J. Balag, D. A. T. Franco, V. G. Miral, V. Reyes, L. J. Tongco, and E. C. R. Lopez, "Recent Advances in Particle Fluidization," in ASEC 2023, MDPI, 2023, p. 62. https://doi.org/10.3390/ASEC2023-15321.

A. O. Bamido, "Design of a fluidized bed reactor for biomass pyrolysis," 2018.

Beheshti SM, Ghassemi H, Shahsavan-Markadeh R (2015) Process simulation of biomass gasification in a bubbling fluidized bed reactor. Energy Convers Manag 94:345–352. https://doi.org/10.1016/j.enconman.2015.01.060

Bhatt MS (2025) Design of combustion chambers in small-sized woodburning stoves. Res Ind 3:1

C. Birzer et al., "An analysis of combustion from a top-lit up-draft (TLUD) cookstove," J. Humanit. Eng., vol. 2, no. 1, 2019.

Boafo-Mensah G, Darkwa KM, Laryea G (2020) Effect of combustion chamber material on the performance of an improved biomass cookstove. Case Stud Therm Eng 21:100688. https://doi.org/10.1016/j.csite.2020.100688

Cáceres-Martínez LE, Guío-Pérez DC, Rincón-Prat SL (2023) Significance of the particle physical properties and the Geldart group in the use of correlations for the prediction of minimum fluidization velocity of biomass–sand binary mixtures. Biomass Convers Biorefinery 13(2):935–951. https://doi.org/10.1007/s13399-020-01189-9

Champion WM et al (2021) Cookstove emissions and performance evaluation using a new ISO protocol and comparison of results with previous test protocols. Environ Sci Technol 55(22):15333–15342. https://doi.org/10.1021/acs.est.1c03390

Commeh MK, Agyei-Agyemang A, Tawiah PO, Asaaga BA (2022) CFD analysis of a flat-bottom institutional cookstove. Sci Afr 16:e01117. https://doi.org/10.1016/j.sciaf.2022.e01117

P. Davenport, Z. Ma, W. Nation, J. Schirck, A. Morris, and M. Lambert, (2022) "Thermal stability of silica for application in thermal energy storage," presented at the SOLARPACES 2020: 26th International Conference on Concentrating Solar Power and Chemical Energy Systems, Freiburg, Germany, p. 160003. https://doi.org/10.1063/5.0085641.

Deng L, Torres-Rojas D, Burford M, Whitlow TH, Lehmann J, Fisher EM (2018) Fuel sensitivity of biomass cookstove performance. Appl Energy 215:13–20. https://doi.org/10.1016/j.apenergy.2018.01.091

Dhakare S, Wathore R, Bherwani H, Gupta A, Dhoble AS, Labhasetwar N (2025) Design optimization of an improved mud cookstove using computational fluid dynamics. Combust Sci Technol 197(10):2391–2413. https://doi.org/10.1080/00102202.2024.2317870

Dran, "Ultimate-and-proximate-analysis-of-wood-and-charcoal-used.png (646×517)." Accessed: Mar. 10, 2025. [Online]. Available: https://www.researchgate.net/profile/P-Abdul-Salam/publication/223040081/figure/tbl1/AS:688078561746944@1541062121033/Ultimate-and-proximate-analysis-of-wood-and-charcoal-used.png

Duan L, Lu D (2025) Fluidized Bed Reactors for Carbon Capture: A Review of Advancing Combustion and Sorption Techniques for Decarbonization. Springer

Gamal ME, Mohammad A, Abu-Jdayil B, Salem IB (2024) Computational study of gas-solid, two-phase interaction system and particle kinetics establishing 3D analysis. Results Eng 24:103562. https://doi.org/10.1016/j.rineng.2024.103562

Ganguli A, Bhatt V (2023) CFD simulations to study bed characteristics in gas–solid fluidized beds with binary mixtures of Geldart B particles: II quantitative analysis. Front Energy Res. https://doi.org/10.3389/fenrg.2023.1150943

E. Getahun, D. Tessema, and N. Gabbiye, "Design and Development of Household Gasifier Cooking Stoves: Natural Versus Forced Draft," in Advances of Science and Technology, vol. 274, F. A. Zimale, T. Enku Nigussie, and S. W. Fanta, Eds., in Lecture Notes of the Institute for Computer Sciences, Social Informatics and Telecommunications Engineering, vol. 274. Cham: Springer International Publishing, 2019, pp. 298–314. https://doi.org/10.1007/978-3-030-15357-1_25.

González-Vázquez MP, García R, Gil MV, Pevida C, Rubiera F (2018) Comparison of the gasification performance of multiple biomass types in a bubbling fluidized bed. Energy Convers Manag 176:309–323. https://doi.org/10.1016/j.enconman.2018.09.020

Goossens WR (2019) Review of the empirical correlations for the drag coefficient of rigid spheres. Powder Technol 352:350–359

Gosavi S, Kulkarni N, Mathpati CS, Mandal D (2018) CFD modeling to determine the minimum fluidization velocity of particles in gas-solid fluidized bed at different temperatures. Powder Technol 327:109–119. https://doi.org/10.1016/j.powtec.2017.12.026

Grace J, Bi X, Ellis N (2020) Essentials of Fluidization Technology, 1st edn. Wiley

Hayyat U et al (2024) Recent developments and challenges in biomass cookstoves. Energy Rep 12:2193–2208. https://doi.org/10.1016/j.egyr.2024.08.016

Hossain MS et al (2022) Design and Development of Bubbling Fluidized Bed Gasifier for Non-woody Biomass Gasification. Chem Eng Trans 92:289–294. https://doi.org/10.3303/CET2292049

Husain Z, Tiwari SS, Pandit AB, Joshi JB (2020) Computational Fluid Dynamics Study of Biomass Cook Stove—Part 1: Hydrodynamics and Homogeneous Combustion. Ind Eng Chem Res 59(9):4161–4176. https://doi.org/10.1021/acs.iecr.9b03181

Hwangdee P, Junsiri C, Sudajan S, Laloon K (2023) Fuel potential values of biomass charcoal powder. Biomass Convers Biorefinery 13(7):5721–5730. https://doi.org/10.1007/s13399-021-01573-z

Ismail TM (2016) Eulerian – eulerian CFD model on fluidized bed gasifier using coffee husks as fuel. Appl Therm Eng 106:1391–1402. https://doi.org/10.1016/j.applthermaleng.2016.06.102

D. Jani, N. Patel, D. Bhandari, and D. Halpati, "Development of multipurpose cook stove," 2020.

Jetter J et al (2012) Pollutant emissions and energy efficiency under controlled conditions for household biomass cookstoves and implications for metrics useful in setting international test standards. Environ Sci Technol 46(19):10827–10834. https://doi.org/10.1021/es301693f

Kalman H, Matana E (2022) Terminal velocity and drag coefficient for spherical particles. Powder Technol 396:181–190

Khezri R et al (2019) Computational fluid dynamics simulation of gas-solid hydrodynamics in a bubbling fluidized-bed reactor: effects of air distributor, viscous and drag models. Processes 7(8):524. https://doi.org/10.3390/pr7080524

Kong D, Luo K, Wang S, Yu J, Fan J (2022) Particle behaviours of biomass gasification in a bubbling fluidized bed. Chem Eng J 428:131847. https://doi.org/10.1016/j.cej.2021.131847

Kumar U, Agarwal VK (2016) Biomass gasification in a fluidized bed reactor: Hydrodynamics and heat transfer studies. Numer Heat Transf Part Appl 70(5):513–531. https://doi.org/10.1080/10407782.2016.1177340

Kwong KY, Marek EJ (2021) Combustion of biomass in fluidized beds: a review of key phenomena and future perspectives. Energy Fuels 35(20):16303–16334. https://doi.org/10.1021/acs.energyfuels.1c01947

Lahai UM, Ofosu EA, Gyamfi S, Diawuo FA (2022) Technical considerations for the design and selection of improved cookstoves: a review. International Journal of Engineering Trends and Technology 70(12):439–449. https://doi.org/10.14445/22315381/IJETT-V70I12P242

Leckner B (2016) Fluidized Bed Combustion. Reference Module in Chemistry, Molecular Sciences and Chemical Engineering. Elsevier, p B9780124095472122000

Leckner B (2019) "Fluidized Bed Combustion", in Reference Module in Chemistry, Molecular Sciences and Chemical Engineering. Elsevier

Li C, Eri " (2023) Comparison between two Eulerian-Lagrangian methods: CFD-DEM and MPPIC on the biomass gasification in a fluidized bed. Biomass Conversion and Biorefinery 13(5):3819–3836. https://doi.org/10.1007/s13399-021-01384-2

Lubwama M, Yiga VA, Ssempijja I, Lubwama HN (2023) Thermal and mechanical characteristics of local firewood species and resulting charcoal produced by slow pyrolysis. Biomass Convers Biorefinery 13(8):6689–6704. https://doi.org/10.1007/s13399-021-01840-z

Luo Z, Tao W (2017) CFBC and BFBC of low-rank coals. Low-Rank Coals for Power Generation, Fuel and Chemical Production. Elsevier, NY, pp 159–178

Marinos-Kouris D, Maroulis Z (2024) Transport Properties in the Drying of Solids. In: Mujumdar A (ed) Handbook of Industrial Drying, 3rd edn. CRC Press

Memon SA, Jaiswal MS, Jain Y, Acharya V, Upadhyay DS (2020) A comprehensive review and a systematic approach to enhance the performance of improved cookstove (ICS). J Therm Anal Calorim 141(6):2253–2263. https://doi.org/10.1007/s10973-020-09736-2

R. R. Mota, "Design And Construction Of A Fluidized Bed," 2015.

D. F. Mugo, M. F. Wamono, M. J. N. Arineitwe, M. F. Nturanabo, and C. van Tilborg, "Consultants and Acknowledgements," 2016.

Mukhopadhyay S, Masto RE, Tripathi RC, Srivastava NK (2019) Application of Soil Quality Indicators for the Phytorestoration of Mine Spoil Dumps. Phytomanagement of Polluted Sites. Elsevier, pp 361–388. https://doi.org/10.1016/B978-0-12-813912-7.00014-4

H. S. Mukunda and E. Professor, "Progress in Biomass combustion and applications," 2022.

Obi OF, Ezema JC, Okonkwo WI (2020) Energy performance of biomass cookstoves using fuel briquettes. Biofuels 11(4):467–478. https://doi.org/10.1080/17597269.2017.1374769

Okino J, Komakech AJ, Wanyama J, Ssegane H, Olomo E, Omara T (2021) Performance Characteristics of a Cooking Stove Improved with Sawdust as an Insulation Material. J Renew Energy 2021:1–12. https://doi.org/10.1155/2021/9969806

Pang L, Shao Y, Zhong W, Liu H (2021) Experimental study and modeling of oxy-char combustion in a pressurized fluidized bed combustor. Chem Eng J 418:129356

Patel AM, Cocco RA, Chew JW (2021) Key influence of clusters of Geldart Group B particles in a circulating fluidized bed riser. Chem Eng J 413:127386. https://doi.org/10.1016/j.cej.2020.127386

Pundle A, Sullivan B, Means P, Posner JD, Kramlich JC (2019) Predicting and analyzing the performance of biomass-burning natural draft rocket cookstoves using computational fluid dynamics. Biomass Bioenergy 131:105402. https://doi.org/10.1016/j.biombioe.2019.105402

Ranzi E, Faravelli T, Manenti F (2016) Pyrolysis, Gasification, and Combustion of Solid Fuels. Advances in Chemical Engineering, vol 49. Elsevier, pp 1–94

Rao BJM, Rao KVNS, Janardhana GR (2018) CFD analysis of hydrodynamic studies of a bubbling fluidized bed. IOP Conf Ser Mater Sci Eng 330:012090. https://doi.org/10.1088/1757-899X/330/1/012090

Rowe PN, Yates JG (2020) "Fluidized-Bed Reactors", in Chemical Reaction and Reactor Engineering. CRC Press

Sadri Mofakham A, Rasteh M (2023) CFD simulation of gas–solid fluidized bed hydrodynamics; prediction accuracy study. Int J Chem React Eng 21(3):391–407. https://doi.org/10.1515/ijcre-2022-0071

Sahoo P, Sahoo A (2015) A comparative study on the effect of different parameters of CFD modeling for gas-solid fluidized bed. Part Sci Technol 33(3):273–289. https://doi.org/10.1080/02726351.2014.952393

Scala F (2018) Particle agglomeration during fluidized bed combustion: Mechanisms, early detection and possible countermeasures. Fuel Process Technol 171:31–38. https://doi.org/10.1016/j.fuproc.2017.11.001

Sedighi M, Salarian H (2017) A comprehensive review of technical aspects of biomass cookstoves. Renew Sustain Energy Rev 70:656–665. https://doi.org/10.1016/j.rser.2016.11.175

Sen R, Wiwatpanyaporn S, Annachhatre AP (2016) Influence of binders on physical properties of fuel briquettes produced from cassava rhizome waste. Int J Environ Waste Manag 17(2):158. https://doi.org/10.1504/IJEWM.2016.076750

Shabanian J, Chaouki J (2017) Effects of temperature, pressure, and interparticle forces on the hydrodynamics of a gas-solid fluidized bed. Chem Eng J 313:580–590. https://doi.org/10.1016/j.cej.2016.12.061

Shao Y, Li Z, Zhong W, Bian Z, Yu A (2020) Minimum fluidization velocity of particles with different size distributions at elevated pressures and temperatures. Chem Eng Sci 216:115555. https://doi.org/10.1016/j.ces.2020.115555

Still D, Bentson S, Li H (2015) Results of laboratory testing of 15 cookstove designs in accordance with the ISO/IWA tiers of performance. EcoHealth 12(1):12–24. https://doi.org/10.1007/s10393-014-0955-6

D. Still et al., "Clean Burning Biomass Cookstoves 2nd Edition 202," 2021.

Sutar KB, Kohli S, Ravi MR (2017) Design, development and testing of small downdraft gasifiers for domestic cookstoves. Energy 124:447–460. https://doi.org/10.1016/j.energy.2017.02.076

Svidró J, Diószegi A, Svidró JT (2020) The origin of thermal expansion differences in various size fractions of silica sand. Int J Cast Met Res 33(6):242–249. https://doi.org/10.1080/13640461.2020.1838078

D. Sweeney, "Handbook for biomass cookstove research, design and development, A practical guide to implementing recent advances," Glob. Alliance Clean Cookstove MIT -Lab, 2017.

Tanui JK, Kioni PN, Kariuki PN, Ngugi JM (2018) Influence of processing conditions on the quality of briquettes produced by recycling charcoal dust. Int J Energy Environ Eng 9(3):341–350. https://doi.org/10.1007/s40095-018-0275-7

Tariku Woldesemayate A, Atnaw SM (2020) A Review on Design and Performance of Improved Biomass Cook Stoves. In: Habtu NG, Ayele DW, Fanta SW, Admasu BT, Bitew MA (eds) Advances of Science and Technology. Springer International Publishing, Cham, pp 557–565

Vargas-Salgado C, Hurtado-Pérez E, Alfonso-Solar D, Malmquist A (2021) Empirical design, construction, and experimental test of a small-scale bubbling fluidized bed reactor. Sustainability 13(3):1061. https://doi.org/10.3390/su13031061

X. Wang, (2014) "Thermal, physical, and mechanical properties of raw sands and sand cores for aluminum casting,".

Wytrwat T, Yazdanpanah M, Heinrich S (2020) Bubble properties in bubbling and turbulent fluidized beds for particles of Geldart's Group B. Processes 8(9):1098. https://doi.org/10.3390/pr8091098

Yunusa SU et al (2023) Biomass cookstoves: a review of technical aspects and recent advances. Energy Nexus 11:100225. https://doi.org/10.1016/j.nexus.2023.100225

Zhang L, Fu Z, Li J, Wang R, Bi X (2023) A review on multi-solids fluidized beds. Powder Technol 414:118091. https://doi.org/10.1016/j.powtec.2022.118091